The Astrophysical Journal, 954:108 (7pp), 2023 September 10 https://doi.org/10.3847/1538-4357/aceb64

Energy Budget in the Solar Corona

Daniele Telloni[1], Marco Romoli[2,3], Marco Velli[4], Gary P. Zank[5,6], Laxman Adhikari[5], Lingling Zhao[5], Cooper Downs[7], Jasper S. Halekas[8], Jaye L. Verniero[9], Michael D. McManus[10,11], Chen Shi[4], Aleksandr Burtovoi[3], Roberto Susino[1], Daniele Spadaro[12], Alessandro Liberatore[13], Ester Antonucci[1], Yara De Leo[14,15], Lucia Abbo[1], Federica Frassati[1], Giovanna Jerse[16], Federico Landini[1], Gianalfredo Nicolini[1], Maurizio Pancrazzi[1], Giuliana Russano[17], Clementina Sasso[17], Vincenzo Andretta[17], Vania Da Deppo[18], Silvano Fineschi[1], Catia Grimani[19,20], Petr Heinzel[21,22], John D. Moses[23], Giampiero Naletto[24], Marco Stangalini[25], Luca Teriaca[14], Michela Uslenghi[26], Stuart D. Bale[10,11], and Justin C. Kasper[27,28]

[1] National Institute for Astrophysics, Astrophysical Observatory of Torino, Via Osservatorio 20, I-10025 Pino Torinese, Italy; daniele.telloni@inaf.it
[2] University of Florence, Department of Physics and Astronomy, Via Giovanni Sansone 1, I-50019 Sesto Fiorentino, Italy
[3] National Institute for Astrophysics, Astrophysical Observatory of Arcetri, Largo Enrico Fermi 5, I-50125 Firenze, Italy
[4] Earth, Planetary, and Space Sciences, University of California, Los Angeles, CA 90095, USA
[5] Center for Space Plasma and Aeronomic Research, University of Alabama in Huntsville, Huntsville, AL 35805, USA
[6] Department of Space Science, University of Alabama in Huntsville, Huntsville, AL 35805, USA
[7] Predictive Science Inc., San Diego, CA 92121, USA
[8] Department of Physics and Astronomy, University of Iowa, Iowa City, IA 52242, USA
[9] National Aeronautics and Space Administration, Goddard Space Flight Center, Greenbelt, MD 20771, USA
[10] Space Sciences Laboratory, University of California, Berkeley, CA 94720, USA
[11] Physics Department, University of California, Berkeley, CA 94720, USA
[12] National Institute for Astrophysics, Astrophysical Observatory of Catania, Via Santa Sofia 78, I-95123 Catania, Italy
[13] Jet Propulsion Laboratory, California Institute of Technology, Pasadena, CA 91109, USA
[14] Max Planck Institute for Solar System Research, Justus-von-Liebig-Weg 3, D-37077 Göttingen, Germany
[15] University of Catania, Department of Physics and Astronomy, Via Santa Sofia 64, I-95123 Catania, Italy
[16] National Institute for Astrophysics, Astronomical Observatory of Trieste, Località Basovizza 302, I-34149 Trieste, Italy
[17] National Institute for Astrophysics, Astronomical Observatory of Capodimonte, Salita Moiariello 16, I-80131 Napoli, Italy
[18] National Research Council, Institute for Photonics and Nanotechnologies, Via Trasea 7, I-35131 Padova, Italy
[19] University of Urbino Carlo Bo, Department of Pure and Applied Sciences, Via Santa Chiara 27, I-61029 Urbino, Italy
[20] National Institute for Nuclear Physics, Section in Florence, Via Bruno Rossi 1, I-50019 Sesto Fiorentino, Italy
[21] Czech Academy of Sciences, Astronomical Institute, Fričova 298, CZ-25165 Ondřejov, Czech Republic
[22] University of Wrocław, Centre of Scientific Excellence—Solar and Stellar Activity, ul. Kopernika 11, PL-51-622 Wrocław, Poland
[23] National Aeronautics and Space Administration, Headquarters, Washington, DC 20546, USA
[24] University of Padua, Department of Physics and Astronomy, Via Francesco Marzolo 8, I-35131 Padova, Italy
[25] Italian Space Agency, Via del Politecnico snc, I-00133 Roma, Italy
[26] National Institute for Astrophysics, Institute of Space Astrophysics and Cosmic Physics of Milan, Via Alfonso Corti 12, I-20133 Milano, Italy
[27] BWX Technologies, Inc., Washington, DC 20002, USA
[28] Climate and Space Sciences and Engineering, University of Michigan, Ann Arbor, MI 48109, USA
Received 2023 July 11; revised 2023 July 23; accepted 2023 July 24; published 2023 August 28

Abstract

This paper addresses the first direct investigation of the energy budget in the solar corona. Exploiting joint observations of the same coronal plasma by Parker Solar Probe and the Metis coronagraph aboard Solar Orbiter and the conserved equations for mass, magnetic flux, and wave action, we estimate the values of all terms comprising the total energy flux of the proton component of the slow solar wind from 6.3 to 13.3 $R_\odot$. For distances from the Sun to less than 7 $R_\odot$, we find that the primary source of solar wind energy is magnetic fluctuations including Alfvén waves. As the plasma flows away from the low corona, magnetic energy is gradually converted into kinetic energy, which dominates the total energy flux at heights above 7 $R_\odot$. It is found too that the electric potential energy flux plays an important role in accelerating the solar wind only at altitudes below 6 $R_\odot$, while enthalpy and heat fluxes only become important at even lower heights. The results finally show that energy equipartition does not exist in the solar corona.

Unified Astronomy Thesaurus concepts: Magnetohydrodynamics (1964); Alfven waves (23); Space plasmas (1544); Interplanetary turbulence (830); Solar corona (1483); The Sun (1693); Solar evolution (1492); Solar wind (1534); Solar physics (1476)

1. Introduction

The corona is the tenuous outermost layer of the Sun's atmosphere, shaped by the strong magnetic fields that dominate the energy and pressure density of the plasma (see the review by Antonucci et al. 2020a, and references therein for a comprehensive and exhaustive dissertation on the observation of the solar corona from space). This is where the solar plasma is heated to temperatures above one million kelvin and the solar wind accelerated to supersonic and super-Alfvénic speeds (Hundhausen 1972; Kohl et al. 1998; Aschwanden 2004). Although slow coronal flows may be driven purely by plasma pressure, it is well known that an additional source of energy is required to accelerate the fast

solar wind. It can be released through interchange magnetic reconnection mechanisms between open and closed magnetic field lines (e.g., Fisk 2003; Bale et al. 2023), often associated with sudden reversals of magnetic field direction, known as switchbacks (e.g., Bale et al. 2019; Zank et al. 2020; Telloni et al. 2022b). Alternatively, waves and/or turbulent fluctuations, transported from below into the corona (e.g., Zank et al. 2017, 2018; Telloni et al. 2023a) or generated locally via nonlinear interactions with a minority reflected sunward by strong coronal stratification (e.g., Matthaeus et al. 1999; Cranmer et al. 2007; Verdini et al. 2009), may couple to the bulk flow, thus providing an additional term to the wind pressure. In any case, whatever physical processes heat and accelerate the coronal plasma, it is now well established that the source of energy that powers the fast solar wind is provided by the magnetic field.

Nonetheless, the solar corona is the site of a variety of dynamic processes involved in the acceleration of the solar wind. To quantify their various contributions to driving coronal outflows, the energy budget in the corona, i.e., the different forms of solar wind energy flux, needs to be investigated. Such a study has so far been precluded due to the lack or limited availability in the corona of measurements of crucial quantities such as the magnetic field, the temperature tensor of the different species comprising the coronal plasma (i.e., protons, electrons, alpha particles, and minor ions), and the heat flux. Recently, however, a joint remote and local observation of the same coronal plasma volume has allowed such an analysis to be initiated. On 2022 June 1, Parker Solar Probe (PSP; Fox et al. 2016), during its twelfth perihelion passage, entered the portion of the plane of the sky (POS) observed remotely by the Metis coronagraph (Antonucci et al. 2020b; Fineschi et al. 2020) aboard the Solar Orbiter (SO; Müller et al. 2020) space mission. This allowed the first-ever simultaneous measurement of the large-scale configuration of the corona and its microphysical/kinetic properties, ultimately enabling the establishment of an empirical magnetohydrodynamic (MHD) model of the slow coronal flow, based solely on the solar wind continuity equations, as well as the first observation-based estimate of the energy transfer rate in the corona (Telloni et al. 2023b). The above empirical MHD wind model offers an opportunity to quantify, for the first time, all the different energy contributions in the corona for the slow wind proton flow between 6.3 and 13.3 $R_\odot$. As a result, the questions of what the primary source of energy is in the extended solar corona and how energy is converted from one form to another can be answered.

Similar work has already been carried out in interplanetary space at different distances and latitudes (Meyer-Vernet 2007; McComas et al. 2014; Liu et al. 2021; Verscharen et al. 2021), down to the upper limit of the solar corona (Halekas et al. 2023), albeit not considering all different forms of energy. In the corona, however, this survey is still lacking. The present paper aims to fill this gap and is organized as follows: definition of the various energy flux terms and the different parameters and assumptions involved in their estimation (Section 2), analysis of the contribution of these energy forms to the net coronal balance with increasing distance from the Sun and discussion of the results (Section 3), and concluding remarks (Section 4).

2. Radial Evolution of Contributions to the Solar Wind Energy Flux

The total energy flux F flowing along a flux tube with cross-sectional area $a = fr^2$ (f is the expansion factor at distance r from the Sun) is the sum of six terms that take into account all the different contributions to wind pressure from both plasma and waves. F thus includes the kinetic energy flux F_U, the enthalpy flux F_T, the gravitational F_g and electric F_e potential energy fluxes, the magnetized turbulence energy flux (both magnetic and velocity fluctuations, the general forms of which are expressed in Wang et al. 2022), often approximated as the Alfvén wave energy flux F_w, and finally the heat flux Q; that is, $F = F_U + F_T + F_g + F_e + F_w + Q$. More specifically, considering the solar wind as a single-species fluid (consisting of the main component of protons, and thus excluding electrons, alpha particles, and minor ions), the fluxes of kinetic energy (related to the expansion of the bulk flow) and enthalpy (i.e., the internal energy related to the thermal agitation motions) are given by

$$F_U = \frac{1}{2}\rho U^3 \tag{1}$$

and

$$F_T = \frac{\rho U}{m_p} k_B \left(T_{\perp p} + \frac{3}{2} T_{\parallel p} \right), \tag{2}$$

respectively, where ρ is the plasma mass density, U is the bulk speed of the solar wind, m_p is the proton mass, and k_B is the Boltzmann constant. Considering, to a first approximation, the proton velocity distribution functions (VDFs) as a single bi-Maxwellian, any anisotropy is taken into account in Equation (2) through the inclusion of the proton temperature components perpendicular $T_{\perp p}$ and parallel $T_{\parallel p}$ to the magnetic field $\boldsymbol{B}$ (it is worth noting, however, that the VDF core and beam can have different anisotropies that are not reflected in the total anisotropy, see, e.g., Klein et al. 2021). Under isotropic conditions, $T_{\perp p} = T_{\parallel p} = T_p$, Equation (2) reduces to $F_T = (5/2) k_B T_p \rho U / m_p$. The gravitational potential energy flux, related to the energy required for the plasma to escape from the Sun's gravitational attraction, is expressed as

$$F_g = -\frac{\rho U G M_\odot}{r}, \tag{3}$$

with G being the gravitational constant. To account for the coupling between protons and electrons, the electric potential energy flux is included in the energy budget of the coronal flow. It is given by

$$F_e = \frac{\rho U}{m_p} e\phi, \tag{4}$$

where $e\phi = (2/\alpha + 1) k_B T_e$ is the electric potential at infinity (with $T_e \propto r^{-\alpha}$ being the electron temperature and α the scaling index), derived from the ambipolar electric field in the generalized Ohm's law. The pressure transported upward by magnetic field fluctuations, namely the magnetized turbulence energy flux, contributes to the overall plasma pressure (and thus to the solar wind energy flux). It is here approximated by the Alfvén wave energy flux. Defining $\boldsymbol{u} = \boldsymbol{U} - \langle \boldsymbol{U} \rangle$ and $\boldsymbol{b} = \boldsymbol{B} - \langle \boldsymbol{B} \rangle$ as the velocity and magnetic fluctuations with

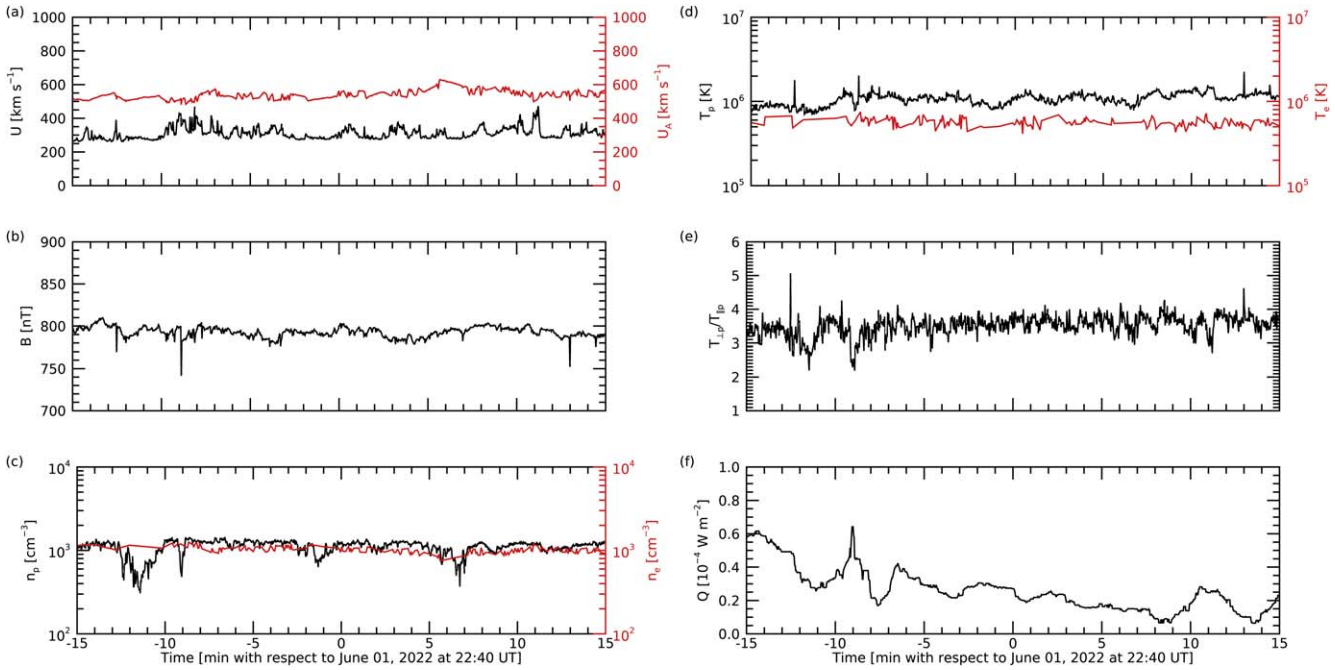

Figure 1. Overview of PSP measurements as the spacecraft entered the POS observed by Metis: (a) bulk-flow and Alfvén speeds (U and U_A, in black and red, respectively), (b) magnetic field intensity B, (c) proton and QTN electron number densities (n_p and n_e, in black and red, respectively), (d) proton and QTN electron temperatures (T_p and T_e, in black and red, respectively), (e) temperature anisotropy $T_{\perp p}/T_{\parallel p}$, and (f) heat flux Q.

respect to the corresponding mean fields ($\langle ... \rangle$ denotes ensemble averages), the outward-propagating modes can be expressed as $\boldsymbol{z}^+ = \boldsymbol{u} + \boldsymbol{b}/\sqrt{\mu\rho}$ (μ is the magnetic permeability) and their energy as $\langle |z^+|^2 \rangle/4$ (Elsässer 1950). Following Chandran et al. (2011), F_w can be thus written as

$$F_w = \left(\frac{3U}{2} + U_A\right)\rho\frac{\langle |z^+|^2 \rangle}{4}, \tag{5}$$

where $U_A = B/\sqrt{\mu\rho}$ is the Alfvén speed. A limitation here is that this expression does not incorporate inward-propagating (see Zhao et al. 2022, showing the presence of inward and outward slab modes) or zero-frequency advected fluctuations, but the corresponding expressions and measurements are more complicated (Wang et al. 2022). The estimate of the fluctuating term can additionally be quite sensitive to residual energy and cross helicity (since this affects the U_A term, for example). Expression (5) provides a reasonable approximation for at least the outward energy flux associated with magnetized coronal turbulence. The exact expression for heat flux is also complicated (e.g., Chandran et al. 2011; Scudder 2015). However, since Q is expected to be negligible compared to the other contributions to the total energy flux above the temperature maximum (namely, for $r > 2$–$4\ R_\odot$, e.g., Antonucci et al. 2005), its free-streaming limit Q_{sat} (Hollweg 1974, 1976), i.e., the heat flux corresponding to a plasma carrying only its own enthalpy, has been used as an estimate here. This expression provides an upper limit, as shown in Chandran et al. (2011). Q can thus be approximated by

$$Q_{sat} = \frac{3}{2}\rho\left(\frac{k_B T_p}{m_p}\right)^{3/2}, \tag{6}$$

where $T_p = (2T_{\perp p} + T_{\parallel p})/3$ is the (average) proton temperature. Finally, it is worth noting that the term associated with the mean background magnetic field, $B^2/(2\mu)$, does not contribute to the energy flux and is therefore not taken into account. At the lowest order and in the steady-state approximation, in fact, the solar wind drags the magnetic field by making it radial, $B \propto r^{-2}$: locally, it corresponds to potential energy density, and therefore neither provides free energy nor contributes to the bulk-flow energy flux. However, it is worth mentioning that the current sheet (where all the energy is stored) acts at least initially as an energy sink, as it arises from the coronal heating via the expansion of the plasma and the opening of previously closed magnetic fields. It therefore acts locally as a source of free energy, allowing for the emission of blobs and some acceleration of the dense plasma sheet, reducing the overall differential between fast and slow wind speeds (see, e.g., Rappazzo et al. 2005; Réville et al. 2020, 2022).

To estimate the different terms involved in the total energy flux and defined in Equations (1)–(6), the radial profiles of ρ, U, B, $\langle |z^+|^2 \rangle$, $T_{\perp p}$, $T_{\parallel p}$, T_p, and T_e have to be inferred or assumed in the solar corona. For this purpose, the joint observations of Metis/SO and PSP of the same volume of solar corona plasma made on 2022 June 1 from 22:25 to 22:55 UT, during the quadrature of the two satellites, have been employed in the computations. The field of view (FOV) of Metis ranged from 6.3 to 13.3 $R_\odot$, with PSP grazing (at about 13.3 $R_\odot$) the outer edge of the portion of the POS imaged with Metis, above its west limb. Some relevant plasma and magnetic field measurements acquired by PSP in the interval of interest are shown in Figure 1. In panels (a)–(f) are the solar wind (black) and Alfvén (red) speeds, magnetic field strength, number densities of protons n_p (black) and electrons n_e (red), proton (black) and electron (red) temperatures, proton temperature anisotropy $T_{\perp p}/T_{\parallel p}$, and heat flux Q, as deduced from the

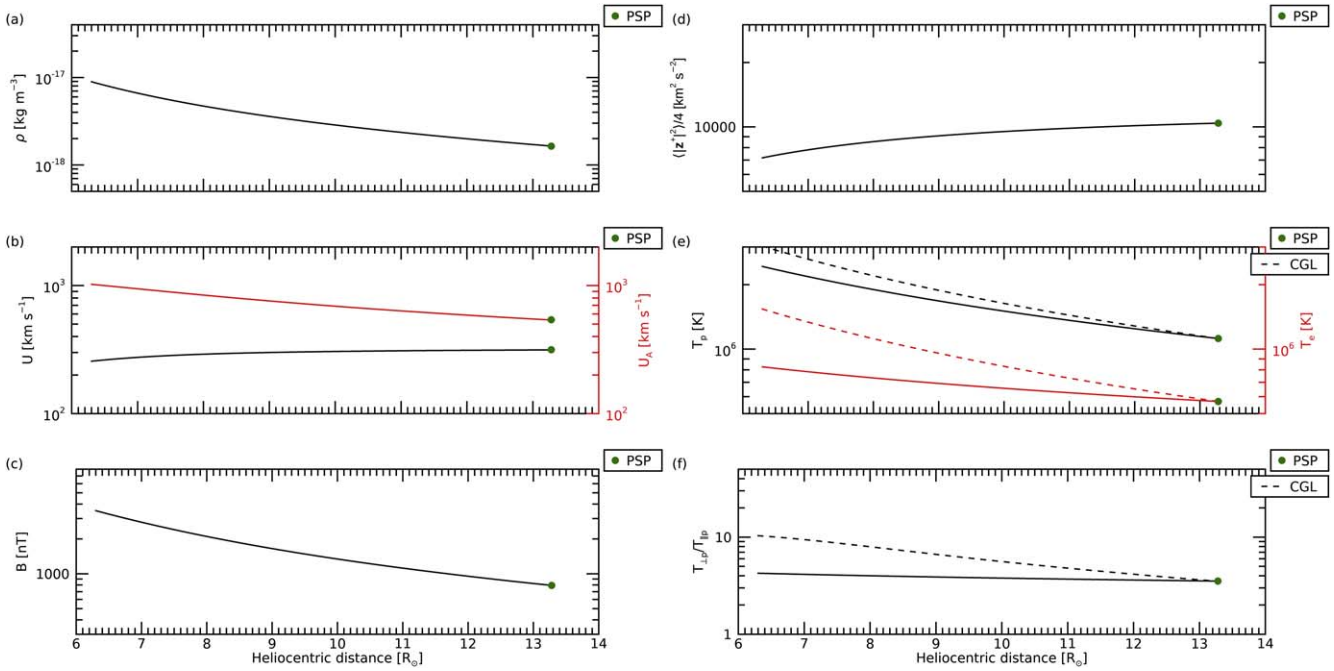

Figure 2. Coronal radial trends in the Metis FOV of (a) plasma mass density, (b) bulk-flow (black) and Alfvén (red) speed, (c) magnetic field strength, (d) outward-propagating Alfvén wave energy, (e) proton (black) and electron (red) temperature, and (f) temperature anisotropy. Dashed curves in (e) and (f) are for profiles obtained in the CGL adiabatic limit. The green dot denotes the PSP-measured reference point for each extrapolated profile.

asymmetry of proton VDFs and computed from bi-Maxwellian core-beam fits (as detailed in Verniero et al. 2022). Data are drawn from the FIELDS experiment (Bale et al. 2016) and the Solar Wind Electrons Alphas and Protons (SWEAP; Kasper et al. 2016) instrument suite. In particular, plasma moments (density, velocity vector, temperature tensor, and heat flux of protons) are provided by the electrostatic Solar Probe Analyzer (SPAN-Ai/SWEAP; Livi et al. 2022), while magnetic field measurements were acquired by the MAG/FIELD fluxgate magnetometer, resampled to the SPAN cadence (1.75 s). Electron number density and temperature are finally obtained from the quasi-thermal noise (QTN) data measured by the radio-frequency spectrometer (RFS/FIELDS; Pulupa et al. 2017). QTN spectroscopy has recently been exploited to infer solar wind electron measurements (Maksimovic et al. 2020; Moncuquet et al. 2020; Zhao et al. 2022).

The plasma volume sampled by PSP belongs to a rather homogeneous slow coronal flow: the average expansion rate is $\langle U\rangle = 315$ km s^{-1} and is less than the Alfvén speed $\langle U_A\rangle = 541$ km s^{-1} (so PSP is effectively in the magnetically dominated corona), and large-scale fluctuations are small. The dip in proton density about 10–15 minutes before quadrature is not real and is due to an excursion of the proton VDF out of the SPAN-Ai FOV (which probably also affects the temperature anisotropy). Indeed, the QTN electron density is steady across the interval and is therefore used in the calculations. It is worth noting that the average measured proton heat flux at 13.3 $R_\odot$ is $\langle Q\rangle = 2.6\times10^{-5}$ W m^{-2}, which is significantly (about two orders of magnitude) smaller than the value obtained in the free-streaming limit, $Q_{\rm sat} = 2.3\times10^{-3}$ W m^{-2}, as expected. Evidence that the proton VDFs are highly anisotropic ($\langle T_{\perp p}/T_{\parallel p}\rangle = 3.6$) during the time interval under study justifies the use of the generalized formula (2) for estimating the proton enthalpy flux.

Averages of the PSP-measured solar wind parameters over the time interval of 30 minutes corresponding to the PSP–SO quadrature[29] serve as reference points at 13.3 $R_\odot$ for their extrapolation downward into the Metis FOV. Following Telloni et al. (2023b), this procedure is carried out by relying on the radial profile of the coronal mass density (inferred from the polarized light images acquired by Metis and calibrated according to De Leo et al. (2023), and shown in Figure 2(a)) and solving the basic conservation equations for the solar wind. More specifically, the coronal flow speed U (black curve in Figure 2(b)) is derived from conservation of mass along the flux tube,

$$U = \frac{\rho^* U^* a^*}{\rho a}, \tag{7}$$

where $f = a/r^2$ was estimated from accurate 3D MHD modeling of the coronal magnetic configuration for the period of interest (developed by Predictive Science Incorporated; Mikić et al. 2018) and found to vary only slightly with distance, i.e., $f\sim 1 \Rightarrow a\sim r^2$ (as expected, since at distances greater than 5 $R_\odot$ the expansion is reasonably purely radial), $\rho = 0.95 m_p n_e$ comes from Metis observations (the factor 0.95 takes into account a helium abundance of 2.5% in a fully ionized plasma (Moses et al. 2020), typical of low-speed streams), and the superscript * refers to the values at the PSP position. Similarly, the coronal magnetic field B (Figure 2(c)), and as a result the Alfvén wave velocity $U_A = B/\sqrt{\mu\rho}$ (red curve in Figure 2(b)), is calculated by conservation of

[29] The first 5 minutes of measurements are excluded from proton velocity and temperature averages to account for the aforementioned SPAN-Ai FOV excursion.

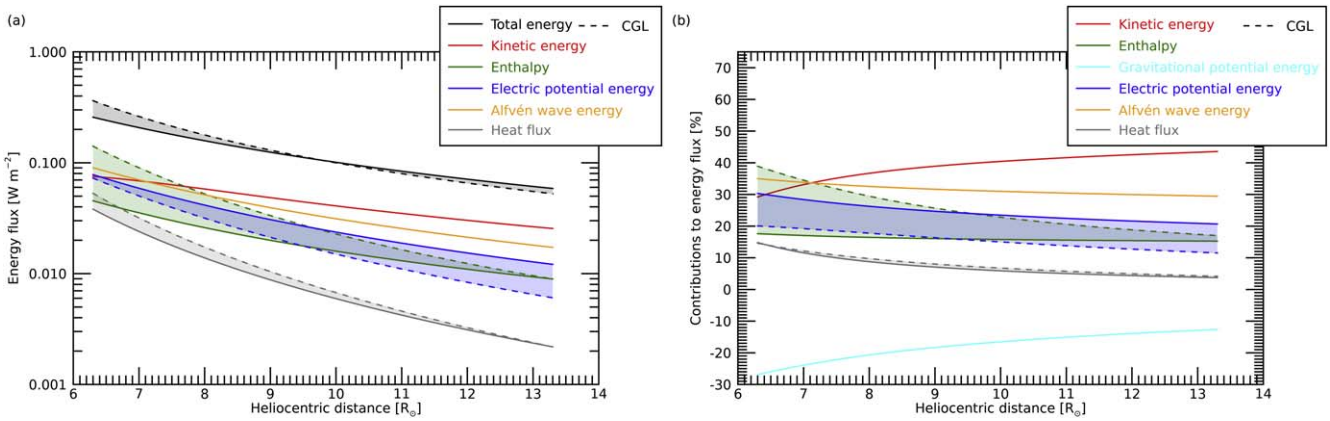

Figure 3. Contributions (a) and fractions (b) of the total energy flux (black), coming from the kinetic energy flux (red), enthalpy flux (green), gravitational (cyan) and electric (blue) potential energy fluxes, Alfvén wave energy flux (yellow), and heat flux (gray). Shaded areas with the same color code indicate the confidence interval for fluxes estimated under different assumptions for coronal quantities (see text for details); the adiabatic approximation is marked by dashed lines.

magnetic flux:

$$B = \frac{B^* a^*}{a}. \tag{8}$$

In the Wentzel–Kramers–Brillouin (WKB) limit (i.e, assuming no dissipation), the radial evolution of the energy associated with upward-propagating Alfvénic fluctuations, $\langle |z^+|^2 \rangle/4$, is obtained in the Metis FOV by conservation of wave action (see, e.g., Velli 1993; Telloni et al. 2023b, for more details):

$$\frac{\langle |z^+|^2 \rangle}{4} = \frac{U U_\mathrm{A}}{(U + U_\mathrm{A})^2} \frac{(U^* + U_\mathrm{A}^*)^2}{U^* U_\mathrm{A}^*} \frac{\langle |z^+|^2 \rangle^*}{4}. \tag{9}$$

Since there are no proton and electron temperature measurements in the 6.3–13.3 $R_\odot$ range studied here (remote spectroscopic observations of the corona are available only further below, while PSP measurements extend just down to 13.3 $R_\odot$), nor MHD-based solutions to propagate PSP measurements backward, some assumptions are required to define the radial profiles of $T_{\perp p}$, $T_{\parallel p}$, T_p, and T_e. One viable approach is to consider that their dependence, as derived from PSP observations in the very inner heliosphere at the lowest limit of 13.3 $R_\odot$, also holds slightly below, down to 6.3 $R_\odot$. Halekas et al. (2023) showed that in the slow solar wind the perpendicular component of the proton temperature scales approximately as $r^{-0.25}$ (in agreement with the results provided by Wu et al. 2020), while the parallel component does not exhibit appreciable variation with heliocentric distance (in accordance with Chandran et al. 2011), at least in the slowest flows. On the other hand, Zhao et al. (2019) found that the near-Sun proton temperature decreases with height as r^{-1}. Finally, based on a statistical survey, Halekas et al. (2022) showed that the electron temperature scales as $r^{-0.5}$ in the low-speed streams. At distances far above the temperature maximum, as in the present case, it is reasonable to assume that the scaling law of proton and electron temperature (along with the corresponding components) does not vary significantly. Therefore, the above literature profiles, which are valid just above the Metis FOV, are also employed in the present work in the range between 6.3 and 13.3 $R_\odot$ (continuous color-coded curves in Figures 2(e) and (f)). Other scaling laws are found in the literature (e.g., Huang et al. 2020), yet those employed in the present analysis represent a lower limit. To account for the uncertainties related to the profiles thus derived and to explore how temperature variability affects the estimate of the energy budget in the solar corona, an upper limit for $T_{\perp p}$, $T_{\parallel p}$, T_p, and T_e, i.e., the expected profiles under the assumption of a spherical adiabatic expansion, is also considered. The conservation of the Chew–Goldberger–Low (CGL; Chew et al. 1956) invariants predicts that $T_{\perp p} \propto B$, $T_{\parallel p} \propto n^2/B^2$, while T_p and T_e scale as $r^{-4/3}$ (dashed color-coded curves in Figures 2(e) and (f)). The complete set of functional forms for estimating the different components of the coronal energy flux are given in Figures 2(a)–(f).

3. Estimate of Energy Flux Terms in the Corona

The energy flux terms so estimated along with (normalized to) the total energy flux are displayed in Figure 3(a) (Figure 3(b)) as a function of heliocentric distance with different colored lines, as reported in the legend. The color-coded shaded areas denote the confidence region of the fluxes due to the use of different solutions for the radial temperature profiles. In particular, the CGL adiabatic limit is indicated by dashed curves.

Figure 3 shows that below ~7 $R_\odot$, the solar wind is driven essentially by magnetized turbulence, here represented by Alfvén waves, which are indeed the primary source of energy (yellow curve) for wind acceleration. In this radial range, indeed, the Alfvén wave energy dominates the energy budget, and its fraction decreases with height as the kinetic energy term increases (Figure 3(b)), thus suggesting an energy transfer from Alfvénic fluctuations to bulk-flow acceleration. During the expansion, a (minority) portion of Alfvén wave energy is therefore converted into gravitational potential energy (cyan curve) as the plasma is carried to greater heights in opposition to the Sun's gravitational force (even if most of the energy needed to overcome the gravitational force is injected at lower heights than those considered in this study). Most of the magnetic turbulence energy, on the other hand, is converted into wind kinetic energy (red curve), whose contribution becomes the most important above ~7 $R_\odot$, gradually increasing up to the upper edge of the corona as observed in this study (i.e., 13.3 $R_\odot$), and thus indicating a gradual (though residual) acceleration of the coronal flow to distances of tens of solar radii (see also Telloni et al. 2021). It is worth mentioning that the Alfvén wave energy flux was calculated in the WKB limit and is therefore to be considered a lower limit. Consequently, Alfvén waves are expected to dominate the total energy flux at

heights somewhat higher than 7 $R_\odot$. These observational results strikingly confirm the theoretical predictions provided by the two-fluid solar wind model by Chandran et al. (2011), where (see their Figure 7) it is shown that the Alfvén wave contribution is the most important up to 8–9 $R_\odot$: beyond, most of the energy flux comes from the bulk-flow kinetic energy term, indicating that the solar wind has largely already been accelerated at these heights. Interestingly, where Alfvén waves begin to govern the plasma flow, the turbulent energy transfer rate peaks (see Figure 2(g) of Telloni et al. 2023b), suggesting that, among the various possible mechanisms, the dissipation of low-frequency turbulence is a credible process for transferring energy from Alfvén waves to solar wind protons (as also shown in Adhikari et al. 2022; Telloni et al. 2022a, 2023a) and thus for heating and accelerating the coronal plasma.

Some contribution to wind driving may also come from the electric potential energy (the third largest energy flux), which furthermore exceeds the kinetic energy term at altitudes slightly less than 6 $R_\odot$ (blue curve). This is in agreement with the results found by Halekas et al. (2023), which show that this form of energy can account for proton acceleration of the lower-speed streams. Enthalpy and heat fluxes (green and gray curves, respectively), on the other hand, are expected to become important only much lower, around 2–4 $R_\odot$, at the temperature maximum (e.g., Antonucci et al. 2005). Only under the assumption of CGL double adiabatic expansion might the enthalpy flux (dashed green curve) also play an important role in accelerating coronal flows in this radial range. It is worth mentioning, however, that the CGL approximation is known not to hold in either the corona or the solar wind, and is only given here as a reference and to provide upper limits for some flux terms. As a final remark, Figure 3 clearly depicts that no form of energy equipartition exists in the corona, as incidentally already predicted theoretically by a number of solar wind models (e.g., Cranmer et al. 2007; Chandran et al. 2011; Zank et al. 2021), which the present empirical results fully confirm.

4. Concluding Remarks

The empirical investigation of the different terms involved in the total energy flux of coronal flows, carried out for the first time in this study, provides a deeper insight into (and confirmation of) the overall picture of the physical processes related to wind acceleration. Synergetic Metis/SO—PSP data and MHD-based extrapolations support a wave-driven solar wind scenario: indeed, magnetized turbulence described here via the Alfvén wave energy flux is identified as the dominant term in accelerating coronal plasma. The electric potential energy also contributes to some extent, providing protons with additional plasma pressure, while other forms of energy may be important only in the lower corona. It turns out that Alfvén wave (and electric potential, secondarily) energy is sufficient to account for the continuous acceleration of the (main) proton component of the slow solar wind. Incidentally, the full conversion of all energy to kinetic energy would give the sampled stream an asymptotic speed of about 450 km s^{-1}.

In a steady state, aF is independent of the heliocentric distance r, that is, the total energy flux is constant along the whole flux tube channeling the coronal flow. In the present study, aF is virtually constant with altitude, varying by less than 1% as the plasma flows away from the Sun over a range of 5 $R_\odot$. On the other hand, a significant (36%) departure from conservation is observed for CGL solutions: this is, however, expected due to the unrealistic assumption (double adiabatic expansion) considered in this approximation. The observed compliance with total energy conservation highlights the absence of significant shear-driven dynamics along adjacent flux tubes (Ruffolo et al. 2020; Telloni et al. 2022a, which could invalidate the assumption of steady-state expansion) and, more importantly, the goodness of the Metis and PSP measurements as well as the soundness of the assumptions employed to infer the radial profiles of the proton temperature components perpendicular and parallel to the magnetic field. Some approximations, however, still remain, such as the WKB limit adopted to compute the Alfvén wave energy in the Metis FOV from the in situ PSP measurements, as well as the fact that we have considered only the primary component of the solar wind (i.e., protons) in the analysis, while neglecting the enthalpy and heat flux also associated with electrons and alpha particles. As PSP enters deeper and deeper into the corona, it will be possible to relax assumptions about the temperature tensor anisotropy and directly measure the energy of Alfvénic fluctuations. For example, during its first close approach to the Sun on 2024 December 24, PSP will be at a distance of just 9.9 $R_\odot$ and in quadrature with Metis, whose FOV will range from 5.7 to 12.2 $R_\odot$: PSP will therefore not just barely graze the Metis FOV as in the present study, but will be fully within it, allowing for a much more accurate investigation. Similarly, a greater level of detail of solar wind energy fluxes will come from including measurements from PSP of electrons and alpha particles in the analysis, i.e., considering a three-fluid solar wind. Specifically, the energy exchange between electrons and ions is clearly very important given the mass difference between electrons and ions and the subsequent electric field set up to precisely fix the neutrality of the corona and the Sun as a whole. However, this is devoted to a future work, when a better data set involving electrons and their probability distribution functions becomes available.

Acknowledgments

Solar Orbiter is a space mission of international collaboration between ESA and NASA, operated by ESA. D.T. was partially supported by the Italian Space Agency (ASI) under contract 2018-30-HH.0. G.P.Z., L.A., and L.-L.Z. acknowledge the partial support of a NASA Parker Solar Probe contract SV4-84017, an NSF EPSCoR RII-Track-1 Cooperative Agreement OIA-2148653, and a NASA IMAP grant through SUB000313/80GSFC19C0027. J.H. acknowledges additional support from the Living With a Star (LWS) program through NASA grant 80NSSC22K1014. J.V. is supported by NASA PSP-GI grant 80NSSC23K0208. P.H. acknowledges support from the grant 22-34841S of the Czech Science Foundation and he was also supported by the program "Excellence Initiative - Research University" for years 2020-2026 at the University of Wrocław, project No. BPIDUB.4610.96.2021.KG. J.H., S.B, and J.K. acknowledge support from NASA through contract NNN06AA01C. The Metis program is supported by ASI under contracts to the National Institute for Astrophysics and industrial partners. Metis was built with hardware contributions from Germany (Bundesministerium für Wirtschaft und Energie through the Deutsches Zentrum für Luft- und Raumfahrt e.V.), the Czech Republic (PRODEX) and ESA. The Metis data analyzed in this paper are available from the PI on request.

Parker Solar Probe data were downloaded from the NASA's Space Physics Data Facility (https://spdf.gsfc.nasa.gov).

ORCID iDs

Daniele Telloni https://orcid.org/0000-0002-6710-8142
Marco Romoli https://orcid.org/0000-0001-9921-1198
Marco Velli https://orcid.org/0000-0002-2381-3106
Gary P. Zank https://orcid.org/0000-0002-4642-6192
Laxman Adhikari https://orcid.org/0000-0003-1549-5256
Lingling Zhao https://orcid.org/0000-0002-4299-0490
Cooper Downs https://orcid.org/0000-0003-1759-4354
Jasper S. Halekas https://orcid.org/0000-0001-5258-6128
Jaye L. Verniero https://orcid.org/0000-0003-1138-652X
Michael D. McManus https://orcid.org/0000-0001-6077-4145
Chen Shi https://orcid.org/0000-0002-2582-7085
Aleksandr Burtovoi https://orcid.org/0000-0002-8734-808X
Roberto Susino https://orcid.org/0000-0002-1017-7163
Daniele Spadaro https://orcid.org/0000-0003-3517-8688
Alessandro Liberatore https://orcid.org/0000-0002-0016-7594
Ester Antonucci https://orcid.org/0000-0003-4155-6542
Yara De Leo https://orcid.org/0000-0003-2426-2112
Lucia Abbo https://orcid.org/0000-0001-8235-2242
Federica Frassati https://orcid.org/0000-0001-9014-614X
Giovanna Jerse https://orcid.org/0000-0002-0764-7929
Federico Landini https://orcid.org/0000-0001-8244-9749
Gianalfredo Nicolini https://orcid.org/0000-0002-9459-3841
Maurizio Pancrazzi https://orcid.org/0000-0002-3789-2482
Giuliana Russano https://orcid.org/0000-0002-2433-8706
Clementina Sasso https://orcid.org/0000-0002-5163-5837
Vincenzo Andretta https://orcid.org/0000-0003-1962-9741
Vania Da Deppo https://orcid.org/0000-0001-6273-8738
Silvano Fineschi https://orcid.org/0000-0002-2789-816X
Catia Grimani https://orcid.org/0000-0002-5467-6386
Petr Heinzel https://orcid.org/0000-0002-5778-2600
John D. Moses https://orcid.org/0000-0001-9670-2063
Giampiero Naletto https://orcid.org/0000-0003-2007-3138
Marco Stangalini https://orcid.org/0000-0002-5365-7546
Luca Teriaca https://orcid.org/0000-0001-7298-2320
Michela Uslenghi https://orcid.org/0000-0002-7585-8605
Stuart D. Bale https://orcid.org/0000-0002-1989-3596
Justin C. Kasper https://orcid.org/0000-0002-7077-930X

References

Adhikari, L., Zank, G. P., Telloni, D., & Zhao, L. L. 2022, ApJL, 937, L29
Antonucci, E., Abbo, L., & Dodero, M. A. 2005, A&A, 435, 699
Antonucci, E., Harra, L., Susino, R., & Telloni, D. 2020a, SSRv, 216, 117
Antonucci, E., Romoli, M., Andretta, V., et al. 2020b, A&A, 642, A10
Aschwanden, M. J. 2004, Physics of the Solar Corona: An Introduction with Problems and Solutions (Berlin: Springer)
Bale, S. D., Badman, S. T., Bonnell, J. W., et al. 2019, Natur, 576, 237
Bale, S. D., Drake, J. F., McManus, M. D., et al. 2023, Natur, 618, 252
Bale, S. D., Goetz, K., Harvey, P. R., et al. 2016, SSRv, 204, 49
Chandran, B. D. G., Dennis, T. J., Quataert, E., & Bale, S. D. 2011, ApJ, 743, 197
Chew, G. F., Goldberger, M. L., & Low, F. E. 1956, RSPSA, 236, 112
Cranmer, S. R., van Ballegooijen, A. A., & Edgar, R. J. 2007, ApJS, 171, 520
De Leo, Y., Burtovoi, A., Teriaca, L., et al. 2023, A&A, in press
Elsässer, W. M. 1950, PhRv, 79, 183
Fineschi, S., Naletto, G., Romoli, M., et al. 2020, ExA, 49, 239
Fisk, L. A. 2003, JGRA, 108, 1157
Fox, N. J., Velli, M. C., Bale, S. D., et al. 2016, SSRv, 204, 7
Halekas, J. S., Bale, S. D., Berthomier, M., et al. 2023, ApJ, 952, 26
Halekas, J. S., Whittlesey, P., Larson, D. E., et al. 2022, ApJ, 936, 53
Hollweg, J. V. 1974, JGR, 79, 3845
Hollweg, J. V. 1976, JGR, 81, 1649
Huang, J., Kasper, J. C., Vech, D., et al. 2020, ApJS, 246, 70
Hundhausen, A. J. 1972, Coronal Expansion and Solar Wind (Berlin: Springer)
Kasper, J. C., Abiad, R., Austin, G., et al. 2016, SSRv, 204, 131
Klein, K. G., Verniero, J. L., Alterman, B., et al. 2021, ApJ, 909, 7
Kohl, J. L., Noci, G., Antonucci, E., et al. 1998, ApJL, 501, L127
Liu, M., Issautier, K., Meyer-Vernet, N., et al. 2021, A&A, 650, A14
Livi, R., Larson, D. E., Kasper, J. C., et al. 2022, ApJ, 938, 138
Maksimovic, M., Bale, S. D., Berčič, L., et al. 2020, ApJS, 246, 62
Matthaeus, W. H., Zank, G. P., Oughton, S., Mullan, D. J., & Dmitruk, P. 1999, ApJL, 523, L93
McComas, D. J., Allegrini, F., Bzowski, M., et al. 2014, ApJS, 213, 20
Meyer-Vernet, N. 2007, Basics of the Solar Wind (Cambridge: Cambridge Univ. Press)
Mikić, Z., Downs, C., Linker, J. A., et al. 2018, NatAs, 2, 913
Moncuquet, M., Meyer-Vernet, N., Issautier, K., et al. 2020, ApJS, 246, 44
Moses, J. D., Antonucci, E., Newmark, J., et al. 2020, NatAs, 4, 1134
Müller, D., St+, Cyr, O. C., Zouganelis, I., et al. 2020, A&A, 642, A1
Pulupa, M., Bale, S. D., Bonnell, J. W., et al. 2017, JGRA, 122, 2836
Rappazzo, A. F., Velli, M., Einaudi, G., & Dahlburg, R. B. 2005, ApJ, 633, 474
Réville, V., Fargette, N., Rouillard, A. P., et al. 2022, A&A, 659, A110
Réville, V., Velli, M., Rouillard, A. P., et al. 2020, ApJL, 895, L20
Ruffolo, D., Matthaeus, W. H., Chhiber, R., et al. 2020, ApJ, 902, 94
Scudder, J. D. 2015, ApJ, 809, 126
Telloni, D., Adhikari, L., Zank, G. P., et al. 2022a, ApJ, 929, 98
Telloni, D., Andretta, V., Antonucci, E., et al. 2021, ApJL, 920, L14
Telloni, D., Antonucci, E., Adhikari, L., et al. 2023a, A&A, 670, L18
Telloni, D., Romoli, M., Velli, M., et al. 2023b, arXiv:2306.10819
Telloni, D., Zank, G. P., Stangalini, M., et al. 2022b, ApJL, 936, L25
Velli, M. 1993, A&A, 270, 304
Verdini, A., Velli, M., & Buchlin, E. 2009, ApJL, 700, L39
Verniero, J. L., Chandran, B. D. G., Larson, D. E., et al. 2022, ApJ, 924, 112
Verscharen, D., Bale, S. D., & Velli, M. 2021, MNRAS, 506, 4993
Wang, B. B., Zank, G. P., Adhikari, L., & Zhao, L. L. 2022, ApJ, 928, 176
Wu, H., Tu, C., Wang, X., He, J., & Yang, L. 2020, ApJL, 904, L8
Zank, G. P., Adhikari, L., Hunana, P., et al. 2017, ApJ, 835, 147
Zank, G. P., Adhikari, L., Hunana, P., et al. 2018, ApJ, 854, 32
Zank, G. P., Nakanotani, M., Zhao, L. L., Adhikari, L., & Kasper, J. 2020, ApJ, 903, 1
Zank, G. P., Zhao, L. L., Adhikari, L., et al. 2021, PhPl, 28, 080501
Zhao, L. L., Zank, G. P., & Adhikari, L. 2019, ApJ, 879, 32
Zhao, L. L., Zank, G. P., Adhikari, L., et al. 2022, ApJL, 934, L36